Electrochemistry Communications 136 (2022) 107207

Contents lists available at ScienceDirect

Electrochemistry Communications

journal homepage: www.elsevier.com/locate/elecom

Porous high-entropy alloys as efficient electrocatalysts for water-splitting reactions

Adewale K. Ipadeola [a,b], Augustus K. Lebechi [b], Lesego Gaolatlhe [b], Aderemi B. Haruna [b], Mira Chitt [c], Kamel Eid [d,*], Aboubakr M. Abdullah [a,*], Kenneth I. Ozoemena [b,*]

[a] Center for Advanced Materials, Qatar University, Doha, P.O. Box 2713, Qatar
[b] Molecular Sciences Institute, School of Chemistry, University of the Witwatersrand, Private Bag 3, PO Wits, Johannesburg 2050, South Africa
[c] Global College of Engineering and Technology (GCET), P.O. Box 2546, CPO Ruwi 112, Sultanate of Oman
[d] Gas Processing Center (GPC), College of Engineering Qatar University, PO Box 2713, Doha, Qatar

ARTICLE INFO

Keywords:
Porous high-entropy alloys
Water-splitting
Water electrolysis
Oxygen evolution reaction (OER)
Hydrogen evolution reaction (HER)

ABSTRACT

Porous high-entropy alloys (HEAs) have emerged as promising electrocatalysts for water-splitting reactions, owing to their rich dissimilar active sites, elemental diversity, and multiple functionalities. The rational design of HEAs for water-splitting attracted great interest in improving their current performance, so it is essential to provide timely updates on this field. This review emphasizes the preparation methods of porous HEAs and the effect of their salient features like high configurational entropy, cocktail effect, lattice distortion, and sluggish diffusion on oxygen evolution reaction (OER) and hydrogen evolution reaction (HER). This mini-review also provides some insights into the current limitations and future perspectives to direct research on the development of ideal HEAs for OER and HER.

1. Introduction

Water-splitting reactions (OER/HER) are highly efficient, green, sustainable energy production and storage sources due to their great energy output and earth-abundant oxygen (O_2) and hydrogen (H_2). [1–3] Ir- and Ru-based catalysts are the most active catalysts for OER, and Pt for HER [4–5]; however, the rarity, intolerable cost, and self-poisoning of these catalysts preclude their practical utilization. [6–8] Unlike noble-metal-based catalysts, transition metals-based catalysts were developed for OER while chalcogenides, perovskite, carbides, and phosphides were used for HER but some carbon-based materials for OER/HER, which are low-cost and earth-abundant. [9–13]

Distinct from traditional metal-based catalysts, HEAs possess many outstanding properties like low-level stacking fault energy, mechanical strength, thermal stability, and stability against radiation and corrosion. [14–18] HEAs have plentiful disparate active sites, elemental diversity, multiple functionalities, lattice distortion, and inherent surface complexity, which tune the adsorption of reactants besides retarding the adsorption of intermediates, thus accelerating water electrolysis kinetics. [14–18] Porous HEAs have the inimitable merits of porous morphologies like excellent surface area, low density, accessible active sites, quick molecule diffusion, and maximized atomic utilization, which tune the adsorption energies for reactants and intermediates during OER/HER. [19–24] The utilization of HEAs in water-splitting has attracted significant attention recently, culminating in 187 articles in total besides 64 articles for only porous HEAs according to the web of science (Fig. 1). Various recent reviews emphasized the rational fabrication of HEAs for OER/HER and other catalytic applications. [25] However, reviews about porous HEAs for complete water-splitting are not yet addressed as far we found.

This review emphasizes the fabrication of porous HEAs for OER/HER with a particular focus on the effects of physiochemical merits (Scheme 1) besides addressing the current challenges on porous HEAs and future research direction to tailor the design of ideal porous HEAs for OER/HER.

2. Fundamental and advantages of HEAs for enhanced OER/HER

The history of crystalline HEAs was dated back to 2004, while amorphous alloys with high mixed entropy are back to the 1990 s. HEAs comprise (≥5 metals) in equiatomic or near equiatomic ratios with concentrations between 5 % and 35 % (Fig. 2a); however, there is no

* Corresponding authors.
E-mail addresses: kamel.eid@qu.edu.qa (K. Eid), bakr@qu.edu.qa (A.M. Abdullah), kenneth.ozoemena@wits.ac.za (K.I. Ozoemena).

https://doi.org/10.1016/j.elecom.2022.107207

Available online 25 January 2022

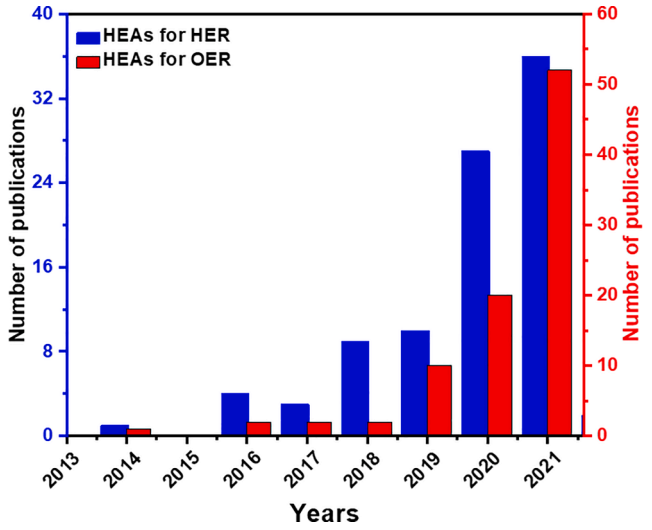

Fig. 1. Number of articles from 2014 to 8th November 2021 obtained from Web of Science using keywords "high-entropy alloys for HER and OER").

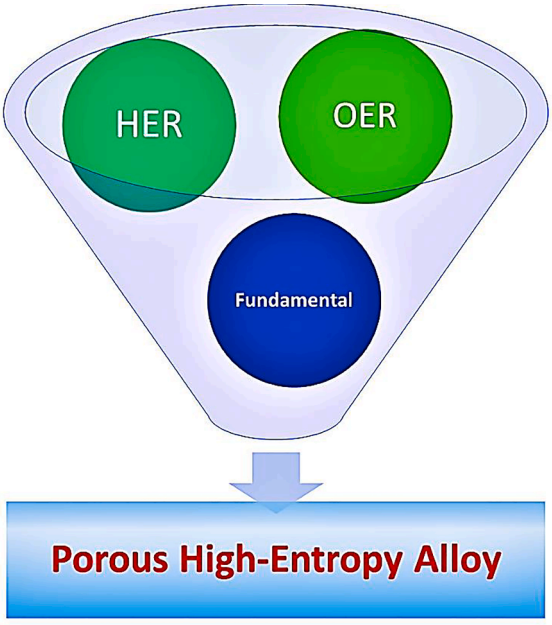

Scheme 1. The overall review outlines.

limit for the concentration of elements. The HEAs are famous for their increased configurational entropy (S) (>1.5R), as given in Eqn. (1). [26]

$$\Delta S_{mix} = -R\sum_{i=1}^{n} c_i \ln c_i = -R\sum_{n}\frac{1}{n}\ln\frac{1}{n} = R\ln n \quad (1)$$

where n is the number of elements and R is the molar gas constant, but there is no maximum number of elements in HEAs, and their effects on OER/HER are still ambiguous. HEAs usually form crystalline face-centered cubic, body-centered cubic, and close-packed hexagonal structures with uniform element distribution due to the high thermal energy of their solid solutions. [15,25,27] But amorphous phases with lattice distortion are formed when there are significant differences in the atom sizes. There are various methods for preparing HEAs like carbothermal shock, electrosynthesis, mechanical milling, solvothermal pyrolysis, wet chemical, pulsed laser ablation, reactive sputter deposition, and dealloying (Table 1). [15,25,27–31] However, other methods like a template, reduction, and polyol may be explored, owing to the tendency of reducing multiple metals simultaneously. [32] HEAs possess various unique merits required for enhanced water electrolysis like phase stability, cocktail effects, slow diffusion, and corrosion resistance (Fig. 2b). [31]

2.1. The high configurational entropy effect

With their mixed multimetallic composition, HEAs have high mixed configurational entropy that increases with increasing the number of components. The high configuration entropy effect is beneficial to produce a stable single-phase solid solution structure of HEAs with excellent OER/HER stability.

2.2. The lattice distortion effect

The dissimilar atomic sizes and electronic configurations allow random occupation in a crystalline and subsequent lattice distortion in HEAs, which endorses the hardness and thermal stability. The tensile lattice strain induced by the lattice distortion upshifts the *d*-band results in a more robust interaction with reactants (O_2/H_2); meanwhile, the compressive strain downshifts the *d*-band to weakening of the interaction during OER/HER.

2.3. The sluggish diffusion effect

The lattice distortion enhances the energy barrier of atomic diffusion, thus decreasing the diffusion effect, while a strike hindrance of atomic diffusion protects against aggregation of HEAs during OER/HER.

2.4. The cocktail effect

The synergism between metals in HEAs promotes the *cocktail* effect, improving the thermo-electric, mechanical, magnetic properties and altering *the d*-band center. Upshifting the *d*-band strengthens the interaction of metals with the O_2/H_2 molecule and weakens the binding energy of OER/HER intermediates. Multiple charge redistribution on the surface of HEAs resulting from different work functions of metals enriches multifunctionality. Despite the unique properties of HEAs, there are some limitations for their use for OER/HER, like lower active sites on the surface and thermodynamic stability at operating conditions. Thermodynamically, high ΔS_{mix} necessitates enthalpy formation (ΔH_{mix}) of intermediates to form a single-phase solution of several elements with low Gibbs free energy ($\Delta G_{mix} \leq 0$, Eqn. (2)).

$$\Delta G_{mix} = \Delta H_{mix} - T\Delta S_{mix} \quad (2)$$

3. Working principles of electrolyzers

The electrolyzer (Fig. 3a) consists of three main parts: anode, cathode, and electrolyte/membrane. The anode and cathode are coated with highly active catalysts to allow water-splitting reactions. Under applied voltage (1.23 V *vs.* RHE), H_2O is cleaved to H_2 (HER) at cathode and O_2 (OER) at anode using linear sweep voltammogram (LSV) test (Fig. 3b). The OER/HER reactions in different electrolytes are shown in Eqns. (3)–(7):

Acidic condition:

$$\text{Anode (OER): } 2H_2O \rightarrow 4H^+ + O_2 + 4e^- \quad (3)$$

$$\text{Cathode (HER): } 4H^+ + 4e^- \rightarrow 2H_2 \quad (4)$$

Alkaline condition:

$$\text{Anode (OER): } 4OH^- \rightarrow 2H_2O + O_2 + 4e^- \quad (5)$$

$$\text{Cathode (HER): } 2H_2O + 4e^- \rightarrow 2H_2 + 4OH^- \quad (6)$$

Overall reaction:

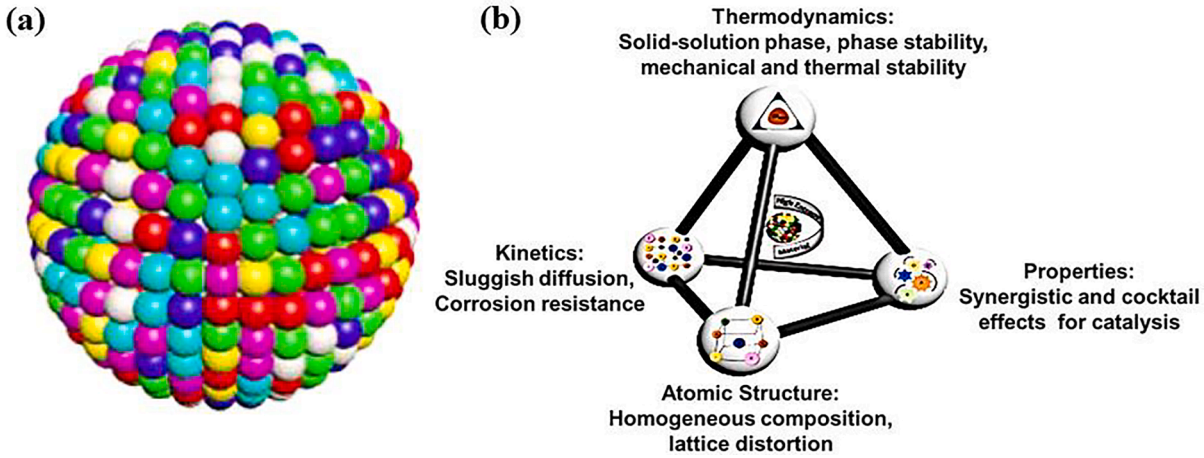

Fig. 2. (a) Typical atomic structure and (b) properties of HEAs. Copyright 2021 Royal Society of Chemistry. [31]

Table 1
The main preparation approaches of HEAs.

Methods	Temperature (°C)/Pressure (atm)	Diameter (nm)	Elements	Substrate
Carbothermal shock	2273/1	3-25	Noble/ non-noble	Carbon
Dealloying	500 /1	2-3	Noble/ non-noble	No-support
Cast cum cryomilling	160 ± 10/Ar	3-14	Noble/ non-noble	No-support
Fast moving bed pyrolysis	1196/Ar	5-50	Noble/ non-noble	Various
Kinetically controlled laser	25/1	2-5	Non-noble	Various
Mechanical alloying	25/1	0.5-20k	Noble/ non-noble	No-support
Solvothermal	200/1	1-100	Noble	Various
Sputtering deposition	25/ultrahigh vacuum	1-4	Noble/ non-noble	Various
Ultrasonication-assisted wet chemistry	25/1	2-80	Noble	Various

$$2H_2O \rightarrow 2H_2 + O_2 \quad (7)$$

The mechanism of HER (Fig. 4a) is classified into three steps with corresponding Tafel slope (b_c), [34] in acid: Volmer ($H^+ + e^- \rightarrow H_{ads}$,$b_c$ = 118.2 mV/dec) involves adsorption of hydrogen ions (H^+) and electrons (e^-) on catalyst's active sites to afford the intermediate adsorption (H_{ads}). Then, the H_{ads} is desorbed to form H_2 by Tafel ($2H_{ads} \rightarrow H_2$; b_c = 29.6 mV/dec) or Heyrovsky ($H_{ads} + H^+ + e^- \rightarrow H_2$; b_c = 39.4 mV/dec). Thus, highly active catalysts must have moderate binding energies with low Δ G_H. OER produces O_2 via several H^+/e^- linked methods (Fig. 4b) involving multi-step reactions via a four-electron pathway ($4e^-$) with a high energy barrier that make OER kinetic very slow with a large overpotential (η). [35] The quest for low-cost and efficient catalysts for OER/HER led to the emergence of HEAs as promising catalysts for both reactions.

4. High-entropy alloys for HER

Various porous HEAs were used as cathodes for HER, like $Ni_{20}Fe_{20}Mo_{10}Co_{35}Cr_{15}$, which had higher activity and stability than Pt sheet with η_{10} 107 mV in H_2SO_4 and 172 mV in KOH. [36] CoCrFeNiAl (HF-HEA_{a2}) obtained by mechanical alloying and spark plasma sintering consolidation, then etching by hydrogen fluoride and activation by cyclic

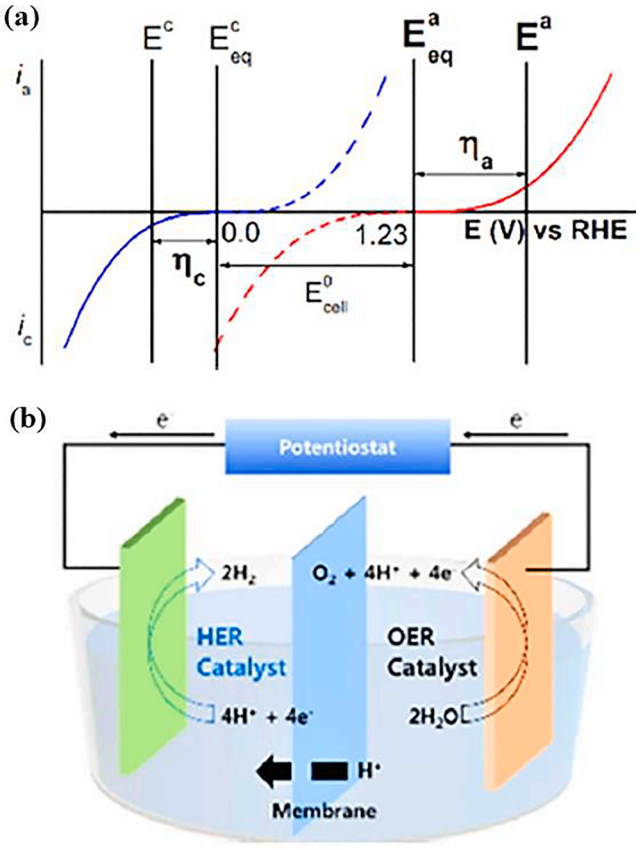

Fig. 3. (a) Overall I-V curve and (b) electrochemical water-splitting. Copyright 2017 KISTI. [33]

voltammetry (CV, 4000 cycles) showed superb HER with η_{10} (73 mV), b_c (39.7 mV/dec), and high stability in H_2SO_4. [37] This was due to the synergistic effects and atomic mixing of its constituent metals. FeCoNiAlTi intermetallics with unusual periodically ($L1_2$-type) ordered structure augmented HER with η_{10} (88.2 mV) and b_c (40.1 mV/dec) akin to Pt-catalysts because the unique $L1_2$-type structure enabled specific site-isolation effect that tuned the H^+/H^* adsorption/desorption. [38]. Monolithic hierarchical CuAlNiMoFe electrode enhanced the HER than CuAlNiFe, CuAlNi, CuAl, Cu, Pt/C/Cu in KOH, as proved by the LSV, EIS, and Tafel plots (Fig. 5a-d). [39] This was due to synergistic effects and hierarchical shape that lowered the H^+ adsorption/desorption,

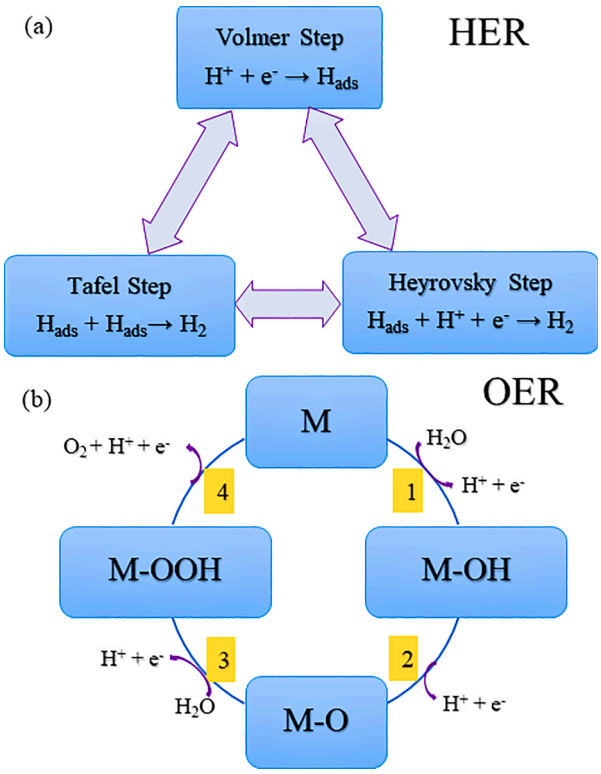

Fig. 4. Mechanisms diagrams of (a) HER and (b) OER.

accelerated HER kinetics, and improved stability for 200 h without structural change (Fig. 5e).

The de-alloyed $Al_{82}Ni_6Co_3Mn_3Y_3Au_3$ with large surface area, lower charge transfer resistance (R_{ct}), η_{10} (24 mV) and b_c (≈ 43 mV/dec) for enhanced HER in acid than Pt/C (η_{10} = 30 mV and b_c = 28 mV/dec). [40] Novel CoCrFeMnNiP formed by a eutectic solvent method had a single metal phosphide phase that increased HER activity with lower η_{10} (136 mV) than its counterparts phosphides and Pt/C. [17] Also, CoCrFeMnNiP gave full water-splitting in KOH at lower voltage (V_{100} = 1.78 V) than Pt/C/IrO_2 ((V_{100}) = 1.87 V). $Pt_{18}Ni_{26}Fe_{15}Co_{14}Cu_{27}$/C synthesized by oil phase method showed HER with low η_{10} (11 mV) and stability in KOH due to its multi-active sites and fast site-to-site e^- that ease H^+ adsorption/desorption as proved by the Density functional theory (DFT). [41] Similarly, PdFeCoNiCu synthesized by oil phase method gave superb alkaline HER with η_{10} (18 mV), b_c (39 mV/dec), high mass activity (6.51 A mg^{-1}_{Pd} at −0.07 V), and durability for 15 days than non-Pd materials. [42] The DFT study showed that Pd and Co were active for initial H_2O cleavage and H_2 formation, respectively, while Ni, Fe, and Cu aided e^- transfer with tuned binding energies of H_{ads}. Nanosponge-like PdPtCuNiP high-entropy metallic glass (HEMG) with ample active sites achieved by surface dealloying had a great HER activity with η_{10} (32 mV) than most presently available catalysts in KOH. [43] The method was scalable and DFT showed that lattice distortion, chemical complexity, and synergism of PdPtCuNiP accelerated H^+ adsorption/desorption. The HER activities of the HEAs are summarized in Table 2. Various porous HEAs with morphologies (Fig. 6a-f) like nanodendrites, nanoporous, nanosponges, and nanosheets were reported for water-splitting.

5. High-entropy alloys for OER

OER is applicable in energy conversion and storage, with IrO_2/RuO_2 being the best catalysts. [46] Lately, HEAs outperformed IrO_2/RuO_2. For example, AlNiCoFeX (X = Mo, Nb, Cr) were designed by controlled integration of metals into an alloy and dealloying their oxidized surface. [45] Amongst the HEAs studied, AlNiCoFeMo showed the best OER compared to its counterparts and RuO_2 due to the impact of synergy into a single-phase structure, giving a valuable structural and chemical degree of freedom. MO_x nanosheet (M = Mn, Fe, Co, and Ni) was grown on MnFeCoNi to form a core–shell structure by CV with an excellent OER. [44] MnFeCoNiCu nanoparticles@N-doped porous carbon on the surface of carbon cloth (HEAN@NPC/CC) nanorods was formed via the in-situ growth of quinary metal–organic frameworks (MOFs) on CC sheets via one-pot solvothermal reaction followed by annealing at different temperatures (400–500 °C) (Fig. 7a-c). [47] HEAN@NPC/CC annealed at 450 °C (HEAN@NPC/CC-450) showed the highest OER activity than its counterparts and RuO_2 as well as FeCoNi/CC, FeCoNiCu/CC, and MnFeCoNi/CC. HEAN@NPC/CC-450 achieved low η_{10} of (302 mV), b_a (83.7 mV/dec) and long-term durability over 20 h for OER (Fig. 7d-i).

AlCrCuFeNi prepared by combining vacuum induction melting, gas atomization, and acidic etching methods enhanced OER activity with η_{10} (270 mV), b_a (77.5 mV/dec), and durability over 35 h compared to RuO_2. [48] $Fe_{29}Co_{27}Ni_{23}Si_9B_{12}$ ribbon made by melt spinning and electrochemical corrosion etching methods had improved OER after etching for 3 h with a lower η_{10} (230 mV) than its crystalline form. [49] The amorphous $Fe_{29}Co_{27}Ni_{23}Si_9B_{12}$ had a reduced interface between the catalyst and the intermediates with optimized Δ G_H. A multilevel structured $(CrFeCoNi)_{97}O_3$ formed by metallurgy method possessed high OER with η_{10} (196 mV), b_a (29 mV/dec), and stability for 120 h, due to the island-like Cr_2O_3 microdomains formation. [50] Porous core–shell $FeCoNiCrNb_{0.5}$ made by the dealloying outperformed other alloys and ceramic catalysts due to its large surface area, fast dynamics, and superb durability. [51]

A high entropy MOF (HE-MOF) synthesized by a solution-phase at room temperature exhibited high OER activity (η_{10} = 245 mV) because of its high configurational entropy. [52] CoFeNiMnMoPi was first prepared by a high-temperature fly-through, which had a higher OER activity, lower η_{10} (270 mV), and b_a (74 mV/dec) than IrO_x. [53] That was because the fly-through allowed metals and phosphorous confinement in one aerosol droplet, *in-situ* oxide-to-phosphate conversion at high temperature, and uniformly mixed multimetallic elements in milliseconds. Ultra-small 3D porous FeCoNiPB/$(FeCoNi)_3O_{4-x}$ (*ca.* 15 nm) formed by air after acid-etching of FeCoNiPB, increased OER activity with low η_{10} (229 mV), η_{100} (406 mV), and good durability due to the rich defect structure. [54] FeNiCoCrMn was prepared via a simple solvothermal process that showed an excellent OER with a small η_{10} (229 mV), and η_{100} (278 mV) with good durability than its subsystems. [55] Flower-like phosphates grown in-situ on porous CoCrFeNiMo to afford P-HF-(CoCrFeNiMo) by hydrothermal-phosphorization gave enhanced OER with low η_{10} (220 mV), b_a (30.3 mV/dec), and superior stability. [21] That was due to abundant OH^-, P-doping, 3D internal connected nanoporous structure, and high conductivity that accelerated charge mobility. The OER activities of HEAs in KOH are summarized in Table 3.

6. Conclusions and future perspectives

This review emphasizes the fabrications of porous HEAs and the effects of their properties on OER and HER. Dealloying is the most common and promising approach for synthesizing HEAs with different morphologies like nanoporous, nanosponges, and nanosheets without substrate. The solvothermal method was also explored to prepare HEAs containing various elements like Pt, Pd, Ru, Rh, and Ir. Various porous HEAs were prepared for HER, which showed η_{10} ranged from 11 to 183 mV, as $Pt_{18}Ni_{26}Fe_{15}Co_{14}Cu_{27}$/C showed the lowest η_{10} of (11 mV). Various porous HEAs were synthesized for OER, which revealed η_{10} ranged from 196 to 302 mV, as $(CrFeCoNi)_{97}O_3$ revealed the lowest η_{10} (196 mV) followed by P-HF-(CoCrFeNiMo) (220 mV). The outstanding OER/HER performances of HEAs aroused from the coupling between the physiochemical merits of HEAs, and the catalytic merits of porous shapes.

In view of future perspectives, the fabrication process of porous HEAs

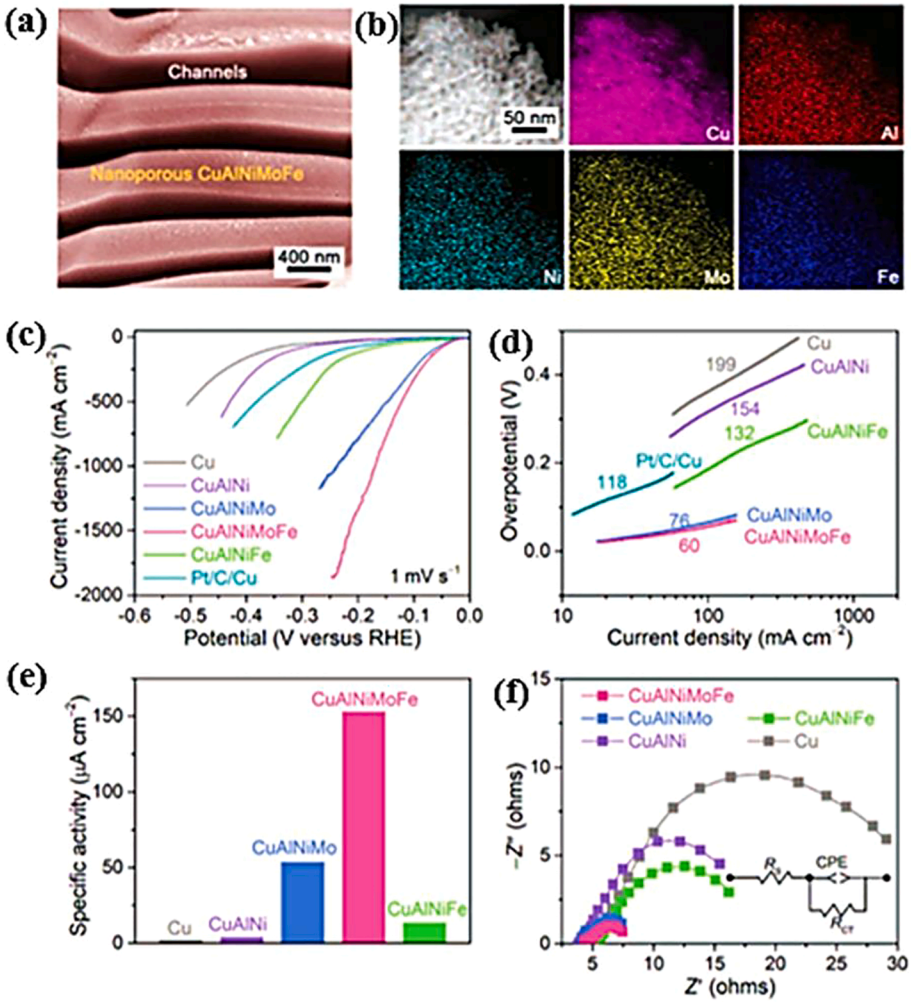

Fig. 5. (a) SEM image, (b) EDS mapping, (c) LSV, (d) Tafel plots, (e) specific activity at $\eta = 240$ mV, and (f) EIS of CuAlNiMoFe and its counterpart. Copyright 2020 Wiley-VCH. [39]

Table 2
Comparison of HER performance of HEAs measured in different electrolytes.

HEAs	Electrolytes	η_{onset} (mV)	η_{10} (mV)	b_c (mV/dec)	Ref.
$Ni_{20}Fe_{20}Mo_{10}Co_{35}Cr_{15}$	0.5 M H_2SO_4	≈41.0	107.0	41.0	[36]
$Ni_{20}Fe_{20}Mo_{10}Co_{35}Cr_{15}$	1.0 M KOH	65.0	172.0	49.0	[36]
CoCrFeNiAl (HF)	0.5 M H_2SO_4	49.0	73.0	39.7	[37]
FeCoNiAlTi	1.0 M KOH	-	88.2	40.1	[38]
CuAlNiMoFe	1.0 M KOH	≈50.0	183.0 @ η_{100}	60.0	[39]
$Al_{82}Ni_6Co_3Mn_3Y_3Au_3$	0.5 M H_2SO_4	0.0	24	43.0	[40]
CoCrFeMnNiP	1.0 M KOH	≈60.0	136	85.5	[17]
$Pt_{18}Ni_{26}Fe_{15}Co_{14}Cu_{27}$/C	1.0 M KOH	0.0	11.0	30.0	[41]
PdFeCoNiCu	1.0 M KOH	0.0	18.0	39.0	[42]
Nanosponge-like PdPtCuNiP	1.0 M KOH	-	32	37.4	[43]

comprised multiple reaction steps, using hazardous chemicals and heating, so they should be simplified. [56] That could be achieved by using combined preparation methods in the presence of various supports. The OER/HER performances of porous HEAs remain unsuitable for practical applications due to improper overpotential, high cost, and complications of the preparation methods. The OER/HER activity and stability of porous HEAs could be enhanced significantly by coupling with other supports like MXenes [57], MOFs, and carbon-based materials [58–62] due to their unique catalytic properties. The DFT and machine learning calculations are needed to predict new HEAs structures and verify their OER/HER activities.

CRediT authorship contribution statement

Adewale K. Ipadeola: Conceptualization, Writing – original draft. **Augustus K. Lebechi:** Data curation. **Lesego Gaolatlhe:** Data curation. **Aderemi B. Haruna:** Data curation. **Mira Chitt:** Data curation. **Kamel Eid:** Writing – review & editing. **Aboubakr M. Abdullah:** Review & supervision. **Kenneth I. Ozoemena:** Review & supervision.

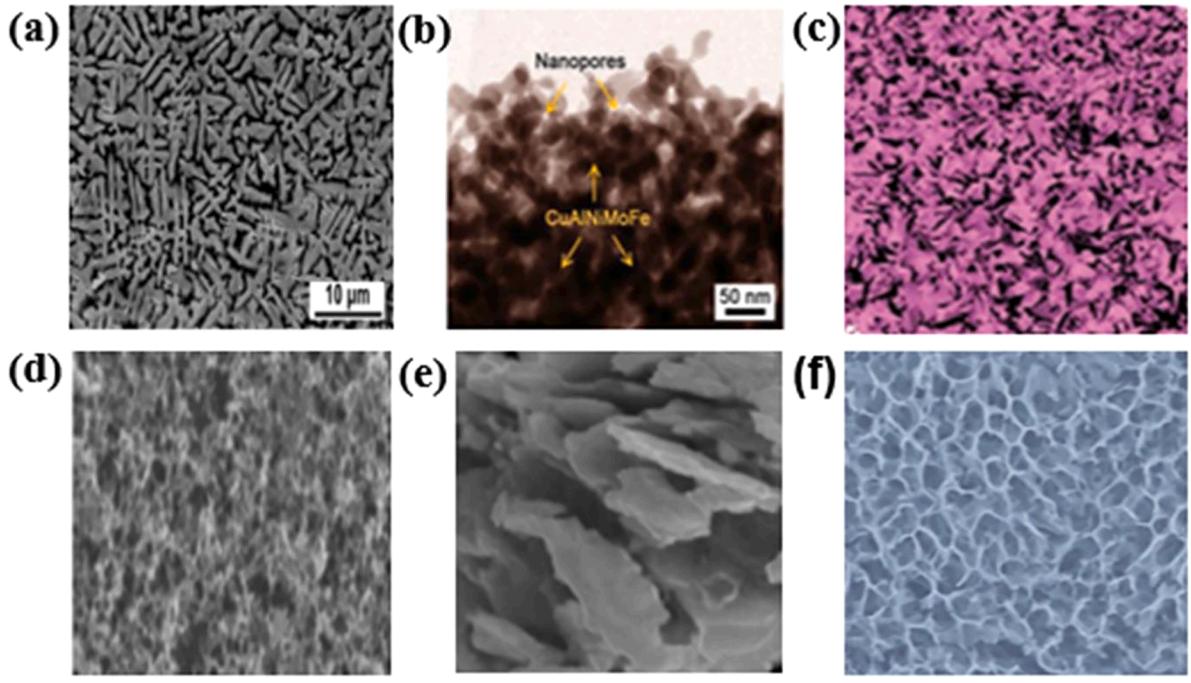

Fig. 6. Morphologies of selected HEA (a) dendrite, [38] (b) nanoporous, [39] (c) nanosponges [43] Copyright 2020 Wiley-VCH, (d) nanocrystals, [40] (e) nanosheets [44] Copyright 2021,2019 Elsevier and (f) nanoporous [45] Copyright 2019 American Chemical Society.

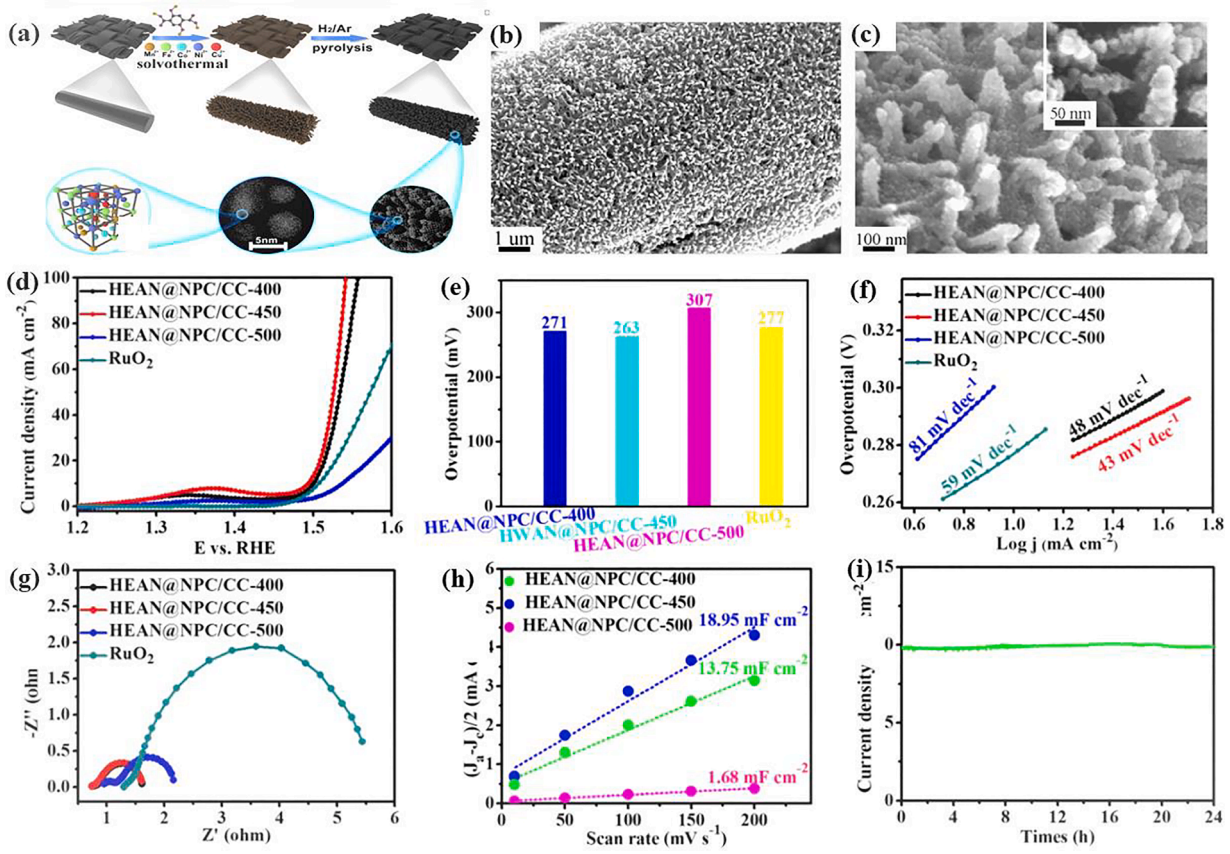

Fig. 7. (a) Preparation scheme, (b,c) FESEM and SEM, (d) LSV, (e) (η_{10}), (f) Tafel slope, (g) EIS of HEAN@NPC/CCs and RuO_2, (h) C_{dl} values of HEAN@NPC/CCs, (i) j-t curve of HEAN@NPC/CC-450. Copyright 2020 Royal Society of Chemistry. [47]

Table 3
Comparison OER performance of HEAs measured in KOH.

HEAs	η_{onset} (mV)	η_{10} (mV)	b_c (mV/dec)	Ref.
AlNiCoFeMo	≈210.0	≈240.0	46.0	[45]
MnFeCoNi	230.0	302.0	83.7	[44]
HEAN@NPC/CC-450	≈240.0	263.0	43.0	[47]
np-AlCrCuFeNi	≈220.0	270.0	77.5	[48]
$Fe_{29}Co_{27}Ni_{23}Si_9B_{12}$ (etched 3h)	≈170.0	230.0	85.0	[49]
$(CrFeCoNi)_{97}O_3$	≈180.0	196	29.0	[50]
$FeCoNiCrNb_{0.5}$	≈260.0	288	27.7	[51]
HE-MOF-RT	≈200.0	245.0	54.0	[52]
CoFeNiMnMoPi	≈160.0	270.0	74.0	[53]
$FeCoNiPB/(FeCoNi)_3O_{4-x}$	-	229.0	146.0	[54]
FeNiCoCrMn-G	≈190.0	229.0	40.0	[55]
P-HF-(CoCrFeNiMo)	≈150.0	220	30.3	[21]

Declaration of Competing Interest

The authors declare that they have no known competing financial interests or personal relationships that could have appeared to influence the work reported in this paper.

Acknowledgement

This work was supported by the International Research Collaboration Co-Fund grant, IRCC-2021-015, and the NRF/DSI/Wits SARChI Chair in Materials Electrochemistry and Energy Technologies (MEET) (NRF UID No. 132739).

References

[1] J. Yang, M.J. Jang, X. Zeng, Y.S. Park, J. Lee, S.M. Choi, Y. Yin, Electrochem. Commun. 131 (2021), 107118.
[2] M.A. Ahsan, T. He, K. Eid, A.M. Abdullah, M.L. Curry, A. Du, A.R. Puente Santiago, L. Echegoyen, J.C. Noveron, J. Am. Chem. Soc. 143 (2021) 1203–1215.
[3] A.K. Ipadeola, P.V. Mwonga, K.I. Ozoemena, Electrochim. Acta 390 (2021), 138860.
[4] A.K. Ipadeola, P.V. Mwonga, S.C. Ray, R.R. Maphanga, K.I. Ozoemena, ChemElectroChem 7 (2020) 4562–4571.
[5] A.K. Ipadeola, N.Z. Lisa Mathebula, M.V. Pagliaro, H.A. Miller, F. Vizza, V. Davies, Q. Jia, F. Marken, K.I. Ozoemena, A.C.S. Appl, Energy Mater. 3 (2020) 8786–8802.
[6] S. Chen, S.S. Thind, A. Chen, Electrochem. Commun. 63 (2016) 10–17.
[7] A.K. Ipadeola, K.I. Ozoemena, RSC Adv. 10 (2020) 17359–17368.
[8] A.K. Ipadeola, P.V. Mwonga, S.C. Ray, R.R. Maphanga, K.I. Ozoemena, Electroanalysis 32 (2020) 3060–3074.
[9] J. Lai, S. Li, F. Wu, M. Saqib, R. Luque, G. Xu, Energy Environ. Sci. 9 (2016) 1210–1214.
[10] K. Eid, M.H. Sliem, A.M. Abdullah, Nanoscale Adv. 3 (2021) 5016–5026.
[11] K. Eid, K.A. Soliman, D. Abdulmalik, D. Mitoraj, M.H. Sleim, M.O. Liedke, H.A. El-Sayed, A.S. AlJaber, I.Y. Al-Qaradawi, O.M. Reyes, Catal, Sci. Technol. 10 (2020) 801–809.
[12] G. Song, Z. Wang, J. Sun, J. Sun, D. Yuan, L. Zhang, Electrochem. Commun. 105 (2019), 106487.
[13] Y.X. Zhang, S.M. Wu, G. Tian, X.F. Zhao, L.Y. Wang, Y.X. Yin, L. Wu, Q.N. Li, Y.X. Zhang, J.S. Wu, Chem. Euro. J., 27 (2021) 14139-14139.
[14] H. Li, J. Lai, Z. Li, L. Wang, Adv. Funct. Mater. 31 (2021) 2106715.
[15] T. Löffler, A. Ludwig, J. Rossmeisl, W. Schuhmann, Angew. Chem. Int. Ed. 60 (2021) 26894–26903.
[16] L. Sharma, N.K. Katiyar, A. Parui, R. Das, R. Kumar, C.S. Tiwary, A.K. Singh, A. Halder, K. Biswas, Nano Res. (2021) 1–8.
[17] X. Zhao, Z. Xue, W. Chen, Y. Wang, T. Mu, ChemSusChem 13 (2020) 2038–2042.
[18] Z.-X. Cai, H. Goou, Y. Ito, T. Tokunaga, M. Miyauchi, H. Abe, T. Fujita, Chem. Sci. 12 (2021) 11306–11315.
[19] H. Son, S. Nam, H. Choi, Powder Metall. 64 (2021) 211–218.
[20] Y.-J. An, L. Zhu, S.-H. Jin, J.-J. Lu, X.-Y. Liu, Metals 9 (2019) 438.
[21] J. Tang, J. Xu, Z. Ye, Y. Ma, X. Li, J. Luo, Y. Huang, J. Alloys Compd. 885 (2021), 160995.
[22] Z. Jin, J. Lv, H. Jia, W. Liu, H. Li, Z. Chen, X. Lin, G. Xie, X. Liu, S. Sun, Small 15 (2019) 1904180.
[23] H.-J. Qiu, G. Fang, Y. Wen, P. Liu, G. Xie, X. Liu, S. Sun, J. Mater. Chem. A 7 (2019) 6499–6506.
[24] G. Fang, J. Gao, J. Lv, H. Jia, H. Li, W. Liu, G. Xie, Z. Chen, Y. Huang, Q. Yuan, Appl. Catal. 268 (2020), 118431.
[25] B. Wang, Y. Yao, X. Yu, C. Wang, C. Wu, Z. Zou, J. Mater. Chem. A 9 (2021) 19410–19438.
[26] Y. Xin, S. Li, Y. Qian, W. Zhu, H. Yuan, P. Jiang, R. Guo, L. Wang, ACS Catal. 10 (2020) 11280–11306.
[27] T.A. Batchelor, J.K. Pedersen, S.H. Winther, I.E. Castelli, K.W. Jacobsen, J. Rossmeisl, Joule 3 (2019) 834–845.
[28] K. Eid, H. Wang, P. He, K. Wang, T. Ahamad, S.M. Alshehri, Y. Yamauchi, L. Wang, Nanoscale 7 (2015) 16860–16866.
[29] K. Eid, H. Wang, V. Malgras, S.M. Alshehri, T. Ahamad, Y. Yamauchi, L. Wang, J. Electroanal. Chem. 779 (2016) 250–255.
[30] S. Lu, K. Eid, Y. Deng, J. Guo, L. Wang, H. Wang, H. Gu, J. Mater. Chem. A 5 (2017) 9107–9112.
[31] A. Amiri, R. Shahbazian-Yassar, J. Mater Chem. A 9 (2021) 782–823.
[32] F. Wu, K. Eid, A.M. Abdullah, W. Niu, C. Wang, Y. Lan, A.A. Elzatahry, G. Xu, A.C. S. Appl, Mater. Interfaces 12 (2020) 31309–31318.
[33] H. Seo, K.H. Cho, H. Ha, S. Park, J.S. Hong, K. Jin, K.T. Nam, J. Korean Ceram. Soc. 54 (2017) 1–8.
[34] X. Zou, Y. Zhang, Chem. Soc. Rev. 44 (2015) 5148–5180.
[35] A.M. Harzandi, S. Shadman, A.S. Nissimagoudar, D.Y. Kim, H.D. Lim, J.H. Lee, M. G. Kim, H.Y. Jeong, Y. Kim, K.S. Kim, Adv. Energy Mater. 11 (2021) 2003448.
[36] G. Zhang, K. Ming, J. Kang, Q. Huang, Z. Zhang, X. Zheng, X. Bi, Electrochim. Acta 279 (2018) 19–23.
[37] P. Ma, M. Zhao, L. Zhang, H. Wang, J. Gu, Y. Sun, W. Ji, Z. Fu, J. Materiomics 6 (2020) 736–742.
[38] Z. Jia, T. Yang, L. Sun, Y. Zhao, W. Li, J. Luan, F. Lyu, L.C. Zhang, J.J. Kruzic, J. J. Kai, Adv. Mater. 32 (2020) 2000385.
[39] R.Q. Yao, Y.T. Zhou, H. Shi, W.B. Wan, Q.H. Zhang, L. Gu, Y.F. Zhu, Z. Wen, X. Y. Lang, Q. Jiang, Adv. Funct. Mater. 31 (2021) 2009613.
[40] X. Liu, S. Ju, P. Zou, L. Song, W. Xu, J. Huo, J. Yi, G. Wang, J.-Q. Wang, J. Alloys Compd. (2021), 160548.
[41] H. Li, Y. Han, H. Zhao, W. Qi, D. Zhang, Y. Yu, W. Cai, S. Li, J. Lai, B. Huang, Nat. Commun. 11 (2020) 1–9.
[42] D. Zhang, Y. Shi, H. Zhao, W. Qi, X. Chen, T. Zhan, S. Li, B. Yang, M. Sun, J. Lai, J. Mater. Chem. A 9 (2021) 889–893.
[43] Z. Jia, K. Nomoto, Q. Wang, C. Kong, L. Sun, L.C. Zhang, S.X. Liang, J. Lu, J. J. Kruzic, Adv. Funct. Mater. 31 (2021) 2101586.
[44] W. Dai, T. Lu, Y. Pan, J. Power Sources 430 (2019) 104–111.
[45] H.-J. Qiu, G. Fang, J. Gao, Y. Wen, J. Lv, H. Li, G. Xie, X. Liu, S. Sun, A.C.S. Mater, Lett. 1 (2019) 526–533.
[46] A.K. Ipadeola, A.B. Haruna, L. Gaolatlhe, A.K. Lebechi, J. Meng, Q. Pang, K. Eid, A. Abdullah, K.I. Ozoemena, ChemElectroChem 8 (2021) 3998–4018.
[47] K. Huang, B. Zhang, J. Wu, T. Zhang, D. Peng, X. Cao, Z. Zhang, Z. Li, Y. Huang, J. Mater. Chem. A 8 (2020) (1947) 11938–11941.
[48] L.-H. Liu, N. Li, M. Han, J.-R. Han, H.-Y. Liang, Rare Metals, 41(20222) 125-131.
[49] H. Wang, R. Wei, X. Li, X. Ma, X. Hao, G. Guan, J. Mater. Sci. Technol. 68 (2021) 191–198.
[50] Z.J. Chen, T. Zhang, X.Y. Gao, Y.J. Huang, X.H. Qin, Y.F. Wang, K. Zhao, X. Peng, C. Zhang, L. Liu, Adv. Mater. 33 (2021) 2101845.
[51] Z. Ding, J. Bian, S. Shuang, X. Liu, Y. Hu, C. Sun, Y. Yang, Adv. Sustain. Syst. 4 (2020) 1900105.
[52] X. Zhao, Z. Xue, W. Chen, X. Bai, R. Shi, T. Mu, J. Mater. Chem. A 7 (2019) 26238–26242.
[53] H. Qiao, X. Wang, Q. Dong, H. Zheng, G. Chen, M. Hong, C.-P. Yang, M. Wu, K. He, L. Hu, Nano Energy 86 (2021), 106029.
[54] R. Wei, K. Zhang, P. Zhao, Y. An, C. Tang, C. Chen, X. Li, X. Ma, Y. Ma, X. Hao, Appl. Surf. Sci. 549 (2021), 149327.
[55] T.X. Nguyen, Y.H. Su, C.C. Lin, J. Ruan, J.M. Ting, Adv. Sci. 8 (2021) 2002446.
[56] K. Li, W. Chen, Mater. Today Energy, 20 (2021) 100638.
[57] B. Salah, K. Eid, A.M. Abdelgwad, Y. Ibrahim, A.M. Abdullah, M.K. Hassan, K.I. Ozoemena, Electroanalysis, doi.org/10.1002/elan.202100269 (2021).
[58] K. Eid, M.H. Sliem, H. Al-Kandari, M.A. Sharaf, A.M. Abdullah, Langmuir 35 (2019) 3421–3431.
[59] K. Eid, M.H. Sliem, A.M. Abdullah, Nanoscale 11 (2019) 11755–11764.
[60] K. Eid, M.H. Sliem, A.S. Eldesoky, H. Al-Kandari, A.M. Abdullah, Int. J. Hydrogen Energy 44 (2019) 17943–17953.
[61] H.I. Abdu, K. Eid, A.M. Abdullah, Z. Han, M.H. Ibrahim, D. Shan, J. Chen, A. A. Elzatahry, X. Lu, Renew. Energy 153 (2020) 998–1004.
[62] H.I. Abdu, K. Eid, A.M. Abdullah, M.H. Sliem, A. Elzatahry, X. Lu, Green Chem. 22 (2020) 5437–5446.